LETTERS
https://doi.org/10.1038/s41564-020-0786-x

nature microbiology

Spermine-mediated tight sealing of the *Magnaporthe oryzae* appressorial pore–rice leaf surface interface

Raquel O. Rocha[1], Christian Elowsky[2], Ngoc T. T. Pham[1] and Richard A. Wilson[1]✉

Cellular adhesion mediates many important plant–microbe interactions. In the devastating blast fungus *Magnaporthe oryzae*[1], powerful glycoprotein-rich mucilage adhesives[2] cement melanized and pressurized dome-shaped infection cells—appressoria—to host rice leaf surfaces. Enormous internal turgor pressure is directed onto a penetration peg emerging from the unmelanized, thin-walled pore at the appressorial base[1–4], forcing it through the leaf cuticle where it elongates invasive hyphae in underlying epidermal cells[5]. Mucilage sealing around the appressorial pore facilitates turgor build-up[2], but the molecular underpinnings of mucilage secretion and appressorial adhesion are unknown. Here, we discovered an unanticipated and sole role for spermine in facilitating mucilage production by mitigating endoplasmic reticulum (ER) stress in the developing appressorium. Mutant strains lacking the spermine synthase-encoding gene *SPS1* progressed through all stages of appressorial development, including penetration peg formation, but cuticle penetration was unsuccessful due to reduced appressorial adhesion, which led to solute leakage. Mechanistically, spermine neutralized off-target oxygen free radicals produced by NADPH oxidase-1 (Nox1)[3,6] that otherwise elicited ER stress and the unfolded protein response, thereby critically reducing mucilage secretion. Our study reveals that spermine metabolism via redox buffering of the ER underpins appressorial adhesion and rice cell invasion and provides insights into a process that is fundamental to host plant infection.

As a group, polyamines are ubiquitous and essential amino acid derivatives, but not all fungi make or require spermine[7]. We were intrigued, therefore, when our preliminary liquid chromatography with multiple reaction monitoring (LC–MRM) mass spectrometry data (confirmed with biological replicates described below) detected spermine in *Magnaporthe oryzae* mycelia. We also noted an earlier report[8] demonstrating that endogenous polyamines in spores, including spermine, are mobilized during appressorium formation. We hypothesized that *M. oryzae* retained the ability to synthesize the dispensable polyamine spermine from the essential polyamine spermidine due to an unspecified role in the rice infection process. To test this, we first sought to identify and characterize the cognate *M. oryzae* spermine synthase-encoding gene *SPS1*.

A relaxed homology search of the *M. oryzae* genome[9] against the yeast spermine synthase protein sequence (SPE4 (also known as YLR146C)) identified the allele MGG_01296 encoding an uncharacterized 594-amino-acid protein with 30% identity to Spe4 and, according to UniProt, with similarity (at the 100% sequence identity threshold) to spermine/spermidine synthase family proteins. Sps1 carries a spermine/spermidine synthase domain, but unlike Spe4, TMHMM predicted that it carries five transmembrane helices. Moreover, PSORTII predicted that the protein is localized to the endoplasmic reticulum (ER) (44%), mitochondria (22%), the vacuole (11%), the nucleus (11%) or the cytoplasm (11%). To study its function, we replaced the first 164 codons of *SPS1* with a selectable marker conferring resistance to sulfonyl urea[10]. Two independent transformations of the Guy11 wild-type (WT) strain yielded two and one Δ*sps1* deletants, respectively . All three Δ*sps1* mutant strains had similar phenotypes, and one deletant was used as the recipient for *SPS1* to generate the add-back Δ*sps1 SPS1* complementation strain. Liquid chromatography–multiple reaction monitoring (LC–MRM) mass spectrometry determined that spermine levels in Δ*sps1* mycelia, when averaged from three independent samples each run in triplicate, were 31.5-fold lower than in WT. By contrast, values for the polyamines ornithine, putrescine, *N*-acetyl putrescine and spermidine were not significantly different (Student's *t*-test $P > 0.05$) between WT and Δ*sps1* samples (Supplementary Table 1). Δ*sps1* sporulation rates on undefined complete media (CM) were indistinguishable from WT (Extended Data Fig. 1a); however, unlike WT and the Δ*sps1 SPS1* complementation strain, Δ*sps1* spores failed to infect rice seedlings when applied to leaves of the susceptible cultivar CO-39 (Fig. 1a). We concluded that *SPS1* encodes the major spermine producer in *M. oryzae* and that *SPS1* and/or spermine is essential for host infection.

Ablating spermine synthase activity did not affect fungal growth on axenic media and, similar to yeast[11], did not result in spermine auxotrophy. That is, the radial growth of Δ*sps1* deletants was similar to WT on both nutrient-rich CM and on defined minimal media without spermine supplementation (Extended Data Fig. 1b). Also, despite being unable to cause disease, the majority of germinating Δ*sps1* spores had, similar to WT, formed appressoria on rice leaf sheath surfaces by 24 h post inoculation (h.p.i.; Extended Data Fig. 1c). However, by 30 h.p.i., about 0.6% of Δ*sps1* appressoria had penetrated leaf cuticles and colonized underlying host cells compared with >90% for the WT (Fig. 1b and Extended Data Fig. 1d). By 44 h.p.i., when WT primary hyphae have expanded into bulbous, branching invasive hyphae (IH) that fill the first invaded cell and are moving into adjacent cells[5], Δ*sps1* primary hyphae or IH were not evident in underlying cells (Fig. 1b). Thus, Δ*sps1* appressoria do not successfully breach rice leaf cuticles.

Although penetration appeared impaired, several lines of evidence suggested that appressorial morphogenesis before penetration was not affected by the loss of *SPS1*. First, superoxide detection

[1]Department of Plant Pathology, University of Nebraska-Lincoln, Lincoln, NE, USA. [2]Department of Agronomy and Horticulture, University of Nebraska-Lincoln, Lincoln, NE, USA. ✉e-mail: rwilson10@unl.edu

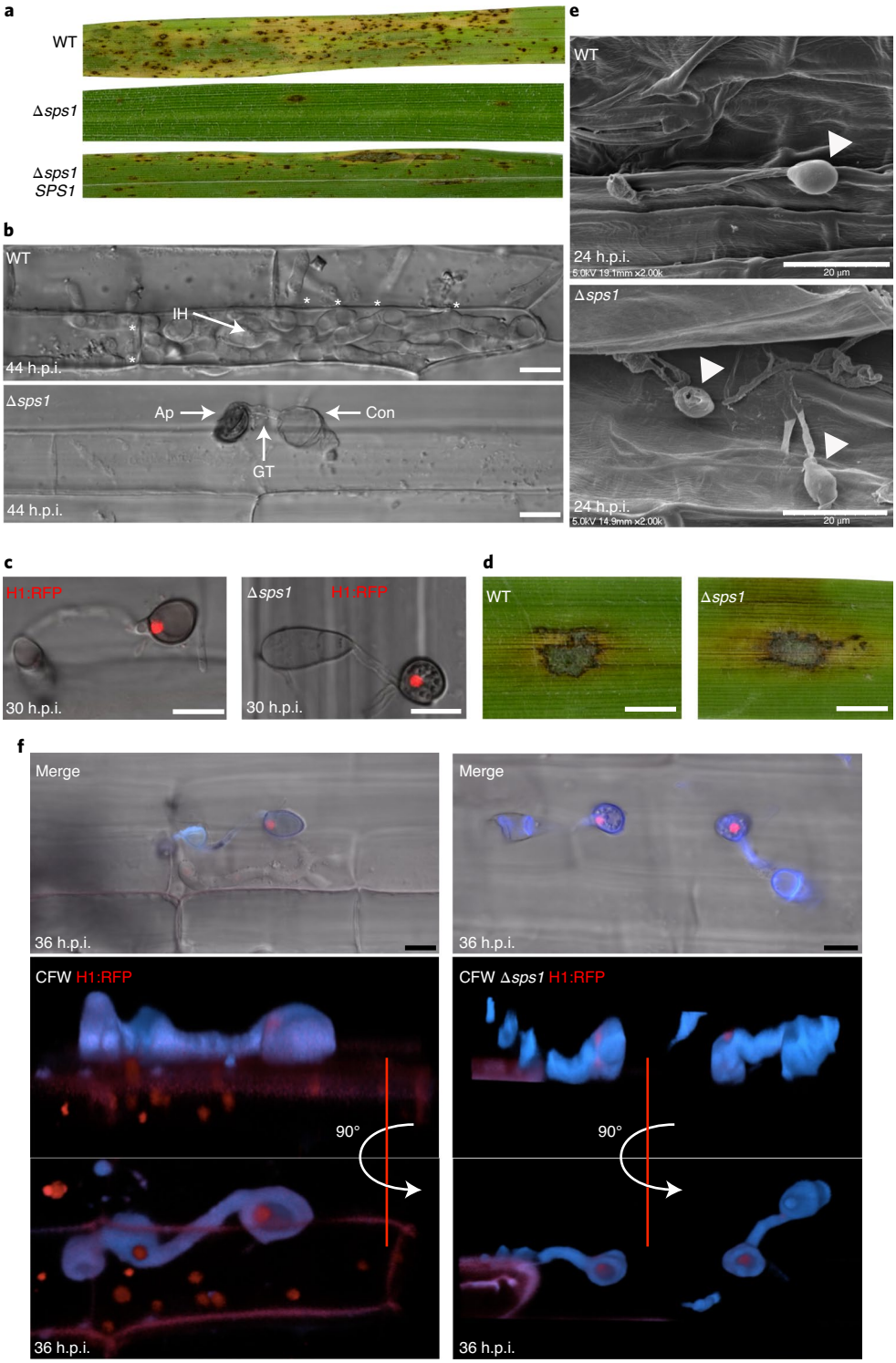

Fig. 1 | *SPS1* is required for appressorial penetration of rice leaf cuticles. a, The Δ*sps1* deletion mutant is nonpathogenic on rice compared with WT and the Δ*sps1 SPS1* complementation strain. A total of 1×10^5 spores per ml of each strain were applied to rice seedlings of the susceptible cultivar CO-39. Images were obtained at 120 h.p.i. **b**, Live-cell imaging of detached rice leaf sheaths inoculated with 1×10^5 spores per ml of the indicated strains and viewed at 44 h.p.i. IH indicates invasive hyphae in the host rice cell. Asterisks indicate IH movement to adjacent cells. Ap, appressoria; Con, conidial spore; GT, germ tube. **c**, Live-cell imaging at 30 h.p.i. of rice leaf sheath surfaces after inoculation with 1×10^5 spores per ml of the indicated strains expressing histone H1 fused to RFP. **d**, The Δ*sps1* mutant strain infected wounded rice leaves. Mycelial plugs of the indicated strains were inoculated onto detached, abraded rice leaves. Leaf infection images were taken at 120 h.p.i. **e**, SEM images of Δ*sps1* and WT appressoria on rice leaf sheath surfaces at 24 h.p.i. Arrowheads indicate appressoria. **f**, Three-dimensional images obtained from live-cell imaging by confocal laser scanning microscopy. Detached rice leaf sheaths were inoculated with 1×10^5 spores per ml of the indicated strains expressing H1:RFP and were stained with CFW at 36 h.p.i. Scale bars, 10 μm (**b**, **c** and **f**) and 0.5 mm (**d**). For **a**–**c** and **f**, images are representative of at least three independent experiments.

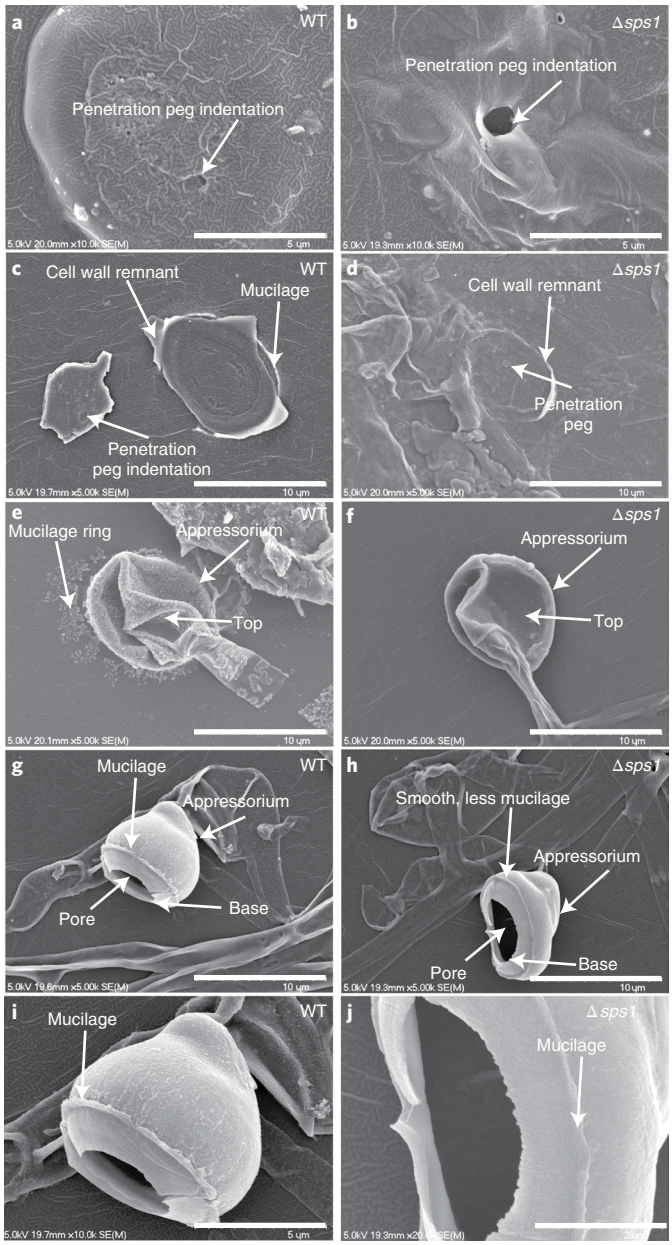

Fig. 2 | *SPS1* is required for appressorial mucilage production and adhesion. a–j, SEM images of WT (left) and Δ*sps1* (right) appressoria and/or associated biological materials (as indicated) formed on cellophane surfaces by 24 h.p.i. with (**a**–**d** and **g**–**j**) or without (**e** and **f**) 30 min of sonication. Images in **i** and **j** are close-ups of the appressoria shown in **g** and **h**, respectively.

by nitrotetrazolium blue chloride showed an oxidative burst at the cell wall of both WT and Δ*sps1* appressoria, which is a requisite for developing a functional appressorium and for forming a penetration peg[3,6] (Extended Data Fig. 2a). Second, similar to WT, germinating Δ*sps1* spores produced inflated, melanized appressoria on rice leaf sheath surfaces with an unmelanized patch covering the pore at the base (Extended Data Fig. 2b). Third, we performed two transformations to disrupt *SPS1* in a *SPS1*$^+$ strain expressing histone H1 fused to red fluorescent protein (RFP)[12]. This yielded one Δ*sps1* H1:RFP strain from each experiment, and both had identical phenotypes that showed germinating Δ*sps1* spores underwent one round of mitosis and autophagic destruction of conidial nuclei, as in WT spores[12–16], which resulted in a single appressorial nucleus on rice leaf sheath surfaces by 30 h.p.i. (Fig. 1c). Furthermore, applying agar plugs of Δ*sps1* mycelia to abraded rice leaf surfaces, which bypasses the need for appressorial penetration, resulted in rice colonization (Fig. 1d). We concluded that *SPS1* and/or spermine is critical for host penetration, but not for infection-related development before or succeeding host penetration.

Scanning electron microscopy (SEM) analyses revealed that by 24 h.p.i., compared with WT, Δ*sps1* appressoria on rice leaf sheath surfaces were not smoothly dome-shaped and had irregular surfaces; indeed, one appeared either ruptured or flipped over (Fig. 1e). Although not evident by confocal microscopy, aberrant Δ*sps1* appressoria were revealed following dimensional scanning of rice leaf sheaths infected with *SPS1*$^+$ H1:RFP (Supplementary Video 1) and Δ*sps1* H1:RFP (Supplementary Video 2) strains after staining with the cell-wall chitin-binding agent calcofluor white (CFW; stills from Supplementary Videos 1 and 2 are shown in Fig. 1f). This analysis also showed that Δ*sps1* germ tubes were not flush with the rice leaf surface and were therefore not firmly attached as for WT germ tubes. Because germ tube adhesion provides one signal for appressorium formation on hydrophobic surfaces, this could account for the reduction in Δ*sps1* appressorium formation rates compared with WT (Extended Data Fig. 1c). Although Δ*sps1* appressoria were misshapen, similar staining of appressorial cell-wall chitin components by CFW indicated that cell wall biosynthesis was probably not perturbed in Δ*sps1* appressoria compared with WT, and cell wall integrity was not compromised. The single Δ*sps1* appressorial nucleus was still present at 36 h.p.i., which suggests that a failure to penetrate the host cuticle arrested the cell cycle at G0, as occurs for WT appressoria on plastic surfaces[15], and halted appressorium morphogenesis at the pre-penetration stage of development. Taken together, these results suggest that the loss of Δ*sps1* appressorial penetration and host cell colonization result from defects in appressorial function but not appressorial development.

On the basis of the previous results, we hypothesized that Δ*sps1* appressoria are noninfective because they did not make penetration pegs. However, by forming appressoria on inductive cellophane surfaces, removing appressoria via sonication at 24 h.p.i. and then examining the underlying substrate by SEM (as previously performed[2,17]), we found holes in the cellophane where penetration pegs had formed under both WT and Δ*sps1* appressoria (Fig. 2a,b). In one case, a Δ*sps1* penetration peg was embedded in the cellophane (Fig. 2d). In many cases, the holes produced by Δ*sps1* penetration pegs were larger than those produced by WT, and we later interpreted this result to indicate that the turgor forces directed onto Δ*sps1* pegs were not uniform because the appressoria were not cemented to the leaf surface by sufficient mucilage (see below), thereby resulting in large movements of Δ*sps1* penetration pegs relative to WT. After sonication, WT appressorial cell-wall remnants remained firmly attached to the substrate surface (as previously reported[2,17]) by a ring of glycoprotein-rich mucilage[2,18] (Fig. 2c). By contrast, considerably less cell wall material remained adhered to cellophane surfaces after Δ*sps1* appressorial removal and no mucilage ring was observed (Fig. 2d). Moreover, SEM of appressoria on cellophane without sonication revealed that after sample preparation, and in contrast to WT, Δ*sps1* appressoria had a very smooth appearance and did not produce observable rings of mucilage around the appressorial base (Fig. 2e,f). Examining appressoria that had been liberated by sonication from cellophane revealed that, similar to WT, Δ*sps1* appressoria had a perfectly formed pore at the base of the appressorium (Fig. 2g–j and Extended Data Fig. 2c), again indicating that cellular processes preceding penetration were not perturbed during Δ*sps1* appressorial morphogenesis. However, whereas WT appressoria retained a rough ring of mucilage around the appressorial pore from where it had been firmly attached to the surface, a similar external ring of mucilage on Δ*sps1* appressoria was smoother and

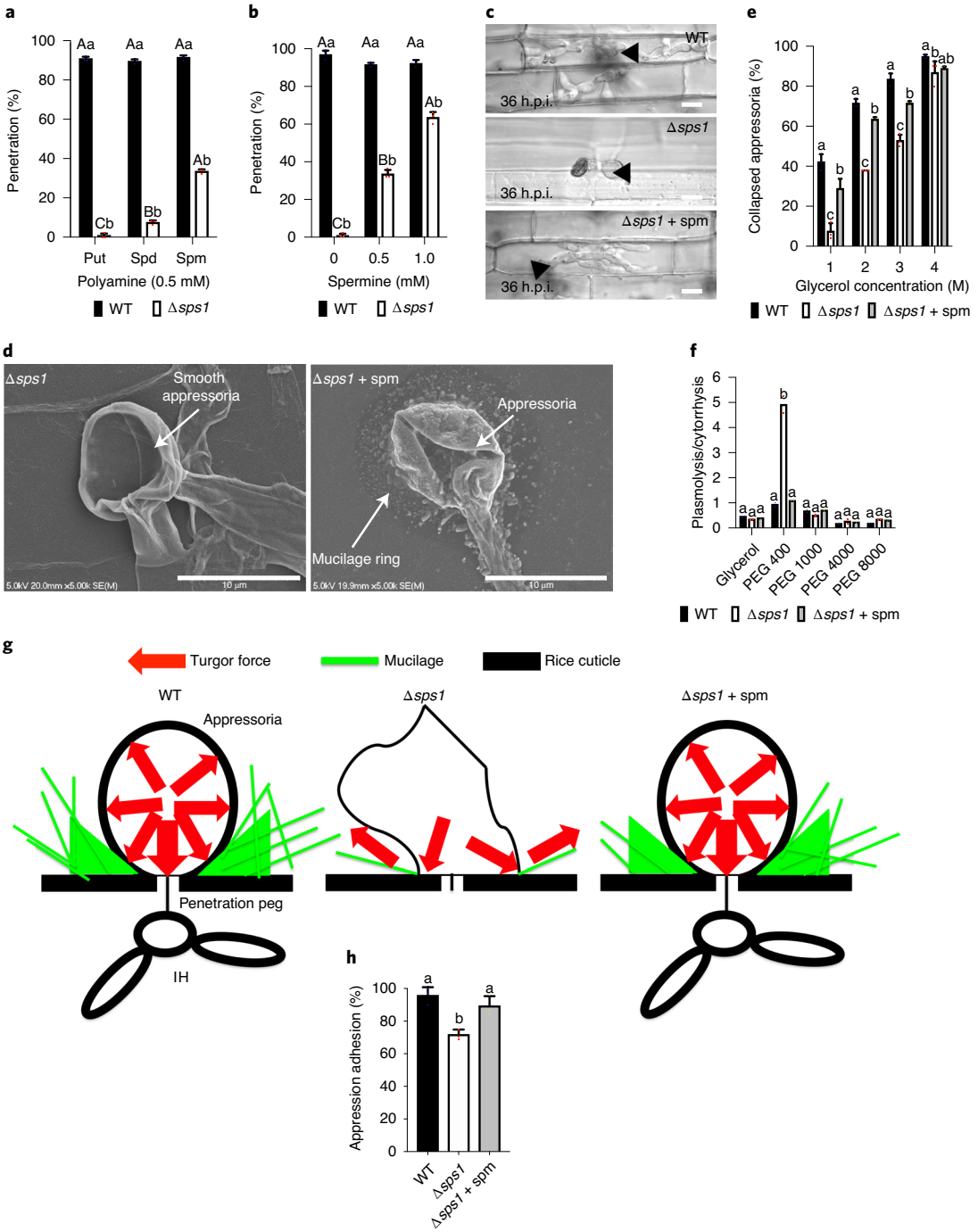

Fig. 3 | Spermine is required for appressorial mucilage production, adhesion and penetration. a,**b**, Penetration rates at 30 h.p.i. for appressoria formed on rice leaf sheath surfaces from spores collected from plates supplemented with the polyamines putrescine (Put), spermidine (Spd) or spermine (Spm) (**a**), and increasing concentrations of spermine (**b**). Values are the mean penetration rates determined for $n = 50$ appressoria, repeated in triplicate. Significant differences of the means comparing WT and Δ*sps1* at a given treatment are denoted by different lowercase letters (two-way ANOVA: **a**, $F_{2,12} = 312.0$, $P < 0.0001$; **b**, $F_{2,12} = 384.7$, $P < 0.0001$). Significant differences of the means within WT (one-way ANOVA: **a**, $F_{2,6} = 2.333$, $P = 0.1780$; **b**, $F_{2,6} = 7.125$, $P = 0.0260$) or within Δ*sps1* (one-way ANOVA: **a**, $F_{2,6} = 670.3$, $P < 0.001$; **b**, $F_{2,6} = 552.6$, $P < 0.001$) at different treatments are denoted by different uppercase letters. **c**, Live-cell imaging of detached rice leaf sheaths inoculated with the indicated strains. Arrowheads indicate appressoria on the surface of the leaf. Scale bar, 10 µm. **d**, SEM images of appressoria on cellophane surfaces. Scale bar, 10 µm. **e**,**f**, Appressorial turgor measurements (**e**) and appressorial porosity measurements (**f**) at 24 h.p.i. on plastic coverslips. Values are the mean of three (**e**) and two (**f**) biological replicates, with **e**ach replicate consisting of observations of $n = 50$ mature appressoria. Significant differences of the means at a given treatment are denoted by different lowercase letters (two-way ANOVA: **e**, $F_{6,24} = 13.58$, $P < 0.0001$; **f**, $F_{8,15} = 109.0$, $P < 0.0001$). **g**, Model showing the effect of spermine loss on appressorial function and morphology. **h**, A 96-well plate-based appressorial adhesion assay, whereby 1×10^4 spores per ml were inoculated into individual wells, repeated in triplicate for each strain. Significant differences of the means are denoted by different lowercase letters (one-way ANOVA: $F_{2,6} = 18.58$, $P = 0.0027$). Rice leaf sheaths (**a**–**c**), cellophane surfaces (**d**) and plastic coverslips (**e** and **f**) were inoculated with 1×10^5 spores per ml of the indicated strains. For **a**, **b**, **e** and **h**, error bars represent the s.d. For **c**–**h**, + spm indicates that the inoculating spores were collected from plates supplemented with 1 mM spermine.

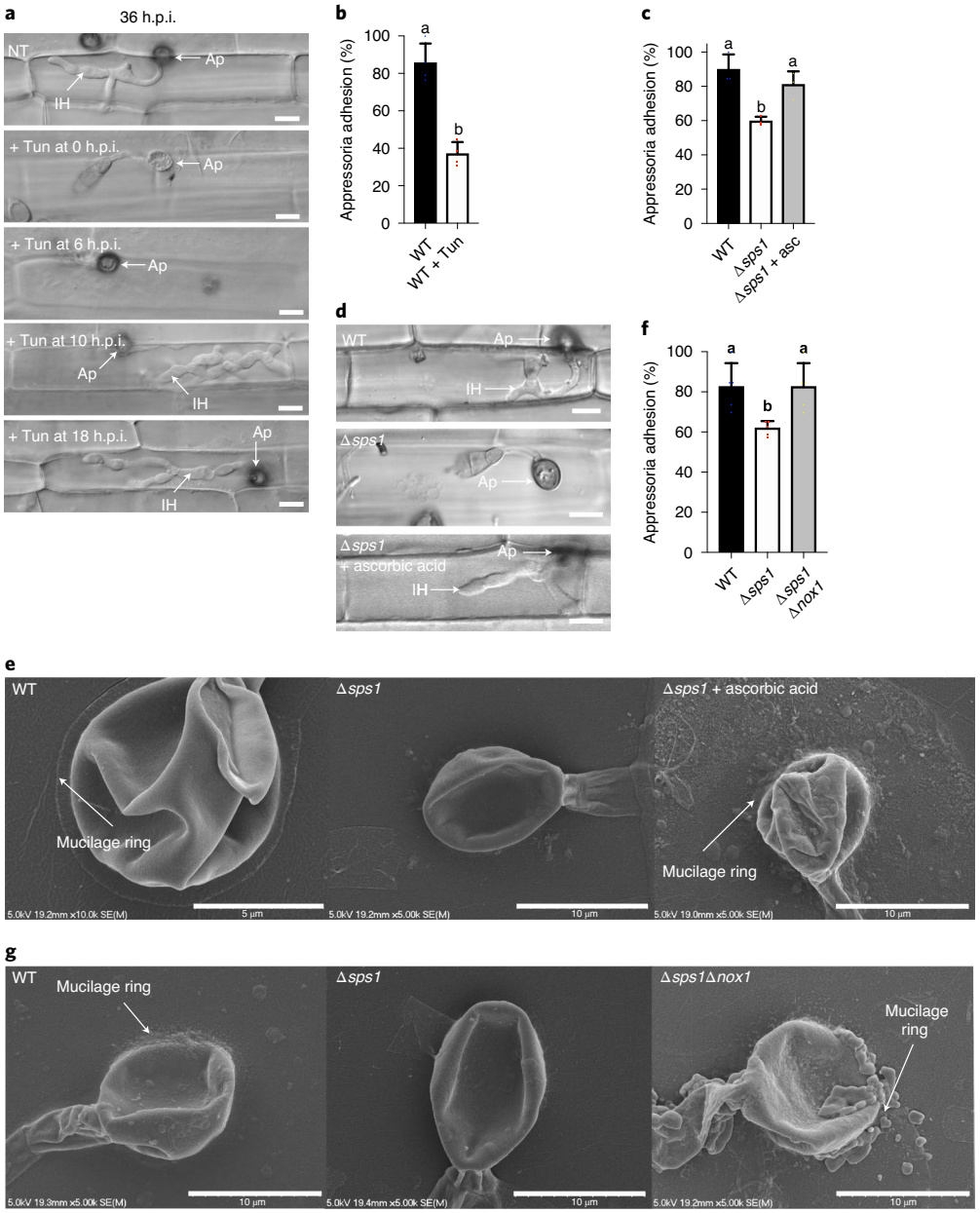

Fig. 4 | Spermine buffers Nox1-generated ROS to mitigate ER stress and promote mucilage secretion. a, The ER stress inducer Tun (5 μg ml^{-1}) was added at the indicated time points to WT spores germinating on detached rice leaf sheath cuticles, and the effect on appressorium formation and penetration was observed by live-cell imaging at 36 h.p.i. Treatment at 6 h.p.i, but not earlier, resulted in melanized appressoria with an unmelanized pore, but no penetration was evident by 36 h.p.i. Ap, appressoria on the leaf surface; IH, invasive hyphae in rice cells; NT, no treatment. **b**, Rates of WT appressorial adhesion in 96-well plates at 24 h.p.i. after germinating spores were treated with Tun (5 μg ml^{-1}) at 6 h.p.i. Tests were repeated in quadruplicate for each treatment. Significant differences of the means are denoted by different lowercase letters (unpaired two-tailed *t*-test: $t = 7.885$, d.f. = 6, $P = 0.0002$). **c**, Adhesion rates after treatment of Δ*sps1* spore suspensions with 2.5 μM ascorbic acid (asc) in 96-well plates. Each treatment was repeated in triplicate. Significant differences of the means are denoted by different lowercase letters (one-way ANOVA: $F_{2,6} = 0.3216$, $P = 0.0051$). **d**, Live-cell imaging at 30 h.p.i. of detached rice leaf sheaths inoculated with the indicated strains. In the lowest panel, Δ*sps1* spores were treated with 0.25 μM ascorbic acid at 0 h.p.i. **e**, SEM images of appressoria on cellophane surfaces showing that by 24 h.p.i., mucilage production can be restored in Δ*sps1* appressoria when inoculating spores are treated with 0.25 μM of the ROS scavenger ascorbic acid. **f**, The Δ*sps1*Δ*nox1* double mutant had appressorial adhesion rates in 96-well plate assays that were comparable to WT. Tests were repeated in quintuplicate. Significant differences of the means are denoted by different lowercase letters (one-way ANOVA: $F_{2,12} = 1.191$, $P = 0.0085$). **g**, SEM images of appressoria on cellophane surfaces at 24 h.p.i. showing that mucilage production can be restored in Δ*sps1* appressoria by the deletion of *NOX1*. For **b**, **c** and **f**, error bars indicate the s.d. Scale bars, 10 μm (**a** and **d**).

diminished (Fig. 2g–j). We concluded that, counter to our expectations, *SPS1* is not required for penetration peg formation or appressorial pore integrity, but is required for mucilage production and tight sealing of the appressorium to the host leaf surface.

Complementing our SEM results, transmission electron microscopy (TEM) analyses of appressoria on plastic coverslips showed that not only were Δ*sps1* appressoria misshapen compared with WT but also that Δ*sps1* appressorial cell walls were significantly

($P = 0.0103$) thinner than WT (Extended Data Fig. 3a,b). In the TEM images, extracellular material, probably mucilage, only sparsely accumulated around Δ*sps1* appressoria compared with WT (Extended Data Fig. 3c).

To determine whether the Δ*sps1* appressorial penetration defect was solely due to the loss of spermine or was instead due to the loss of spermine-independent functions of Sps1, we tested whether spermine could remediate Δ*sps1* appressorial penetration defects. However, as previously reported[8], exogenous polyamine treatments abolished appressorium formation by both WT and Δ*sps1* strains if added before 6 h.p.i., while exogenous spermine did not remediate Δ*sps1* appressorial penetration on detached rice leaf sheaths if added after 6 h.p.i. (Extended Data Fig. 2d). To circumvent this remediation problem, we instead grew strains axenically on plates supplemented with one of the three main polyamines or on increasing concentrations of spermine. Δ*sps1* spores collected from plates supplemented with spermine, but not putrescine or spermidine, formed appressoria that penetrated host cells (Fig. 3a) at a rate that increased with increasing spermine supplementation (Fig. 3b), which then resulted in Δ*sps1* IH in rice cells (Fig. 3c). Importantly, on cellophane, Δ*sps1* spores collected from spermine-supplemented plates elaborated appressoria that produced mucilage similar to WT appressoria (Fig. 3d). These results indicated that spermine is required for appressorial mucilage production. Next, we determined that reduced Δ*sps1* appressorial mucilage production resulted in solute leakage from the pore, and that this defect was remediated when spores were collected from spermine-supplemented plates. Solute leakage was inferred from appressorial turgor and permeability measurements on hard inductive surfaces (plastic cover slips). The results nominally indicated that untreated Δ*sps1* appressoria had both higher internal turgor than WT (as determined by monitoring appressorial collapse rates under increasing external glycerol concentrations; Fig. 3e) and were more permeable to solutes (as determined using polyethylene glycols (PEGs) of different molecular weights; Fig. 3f). These seemingly contradictory results, which suggest that Δ*sps1* appressorial cells are both elevated in internal turgor and more permeable to solutes than WT on hard surfaces, are consistent with glycerol and PEG 400 being exchanged into Δ*sps1* appressoria through unsealed pores, as has been previously described[2] for WT appressoria on soft surfaces. When considered together, we suggest that our results fit the model presented in Fig. 3g and conclude that spermine has a fundamental and sole role in appressorial mucilage production that leads to sufficient adhesion and sealing of the appressorial pore to prevent solute leakage and facilitate turgor-driven breaching of the rice cuticle by the penetration peg. Additional support for this model is presented in Fig. 3h, whereby a 96-well microtitre-plate-based appressorial-adhesion assay[19,20] showed that Δ*sps1* spores from untreated but not from spermine-supplemented plates formed significantly ($P \leq 0.05$) less adhesive appressoria than WT on plastic surfaces.

We next asked whether the role of spermine in appressorial adhesion is specific to *M. oryzae* or more widespread. Previous biochemical analyses of a relatively limited number of fungal species showed that filamentous fungi often do not make spermine, and uncharacterized homologues of the yeast spermine synthase gene *SPE4* are present in the genomes of only a few filamentous fungi[7]. However, Sps1 is a previously undocumented spermine synthase with five transmembrane helices and with low identity to Spe4 outside the spermine-synthase domain. We therefore performed a BLASTP search using the full-length Sps1 amino-acid sequence. The 50 best hits (all filamentous fungi) were retrieved, and the protein sequences were aligned and used to build an unrooted maximum likelihood phylogenetic tree (Extended Data Fig. 4). This tree showed that in addition to a cluster of appressorium-forming species closely related to *M. oryzae*, the majority of fungal species carrying *SPS1* form appressoria or appressoria-like infection structures, including *Magnaporthiopsis poae*, *Gaeumannomyces tritici*, *Fusarium* spp. and *Colletotrichum* spp.; these species, to our knowledge, have not been assessed for spermine production. Together, these results suggest that spermine might be a previously obscured determinant of infection structure adhesion in at least some other important appressoria-forming fungal plant pathogens.

How does spermine mediate mucilage production and appressorial adhesion? To our knowledge, a connection between spermine or other polyamines and mucilage has not been reported for fungi[7] or plants[21], and spermine is not a known component of mucilages. Few studies have examined the adhesives in *M. oryzae* mucilage, which consists of a complex of glycoproteins with mannose sugars[22] in addition to lipids (mostly hexadecanoic and octadecanoic acid) and glycolipids[18]. Antibodies against animal cell-adhesion factors suggest that the glycoproteins vitronectin, fibronectin and laminin, as well as collagen VI and integrin α_3, might be important components of appressorial mucilage[23]. Secreted proteins are glycosylated and folded in the ER, and the ER requires redox buffers to maintain the highly oxidizing environment required for disulfide bond formation and oxidative protein folding[24–26]. The loss of glycosylation and/or protein misfolding in the ER lumen[24,25], the latter often associated with increases in ER reactive oxygen species (ROS)[24,26], results in ER stress, which triggers the unfolded protein response (UPR)[25,26]. We hypothesized that spermine is required during appressorial morphogenesis to buffer oxidative stress in the ER lumen in order to optimize oxidative protein-folding conditions for mucilage production and to prevent ER stress and the UPR. This hypothesis is based on the following reasons: (1) antioxidants relieve UPR[26]; (2) spermine acts as a direct ROS scavenger[27,28]; (3) spermine modulates ER homeostasis and protein folding in the ER[28]; and (4) Sps1 might be localized to the ER. Several other lines of evidence from this current study support our hypothesis. First, UPR and cell-wall integrity pathway genes[29,30] were upregulated in Δ*sps1* mycelia grown in untreated but not spermine-treated media (Extended Data Fig. 5), which indicates that the loss of spermine induces ER stress. Second, inducing ER stress with tunicamycin (Tun)—which inhibits N-linked glycosylation and blocks protein folding and transit through the ER—prevented penetration by WT appressoria on rice leaf sheaths if added by (but not after) 6 h.p.i. (Fig. 4a and quantified in Extended Data Fig. 6a). Furthermore, following Tun treatment of germinating WT spores at 6 h.p.i., the resulting appressoria were melanized and had unmelanized pores similar to untreated appressoria (Fig. 4a). However, appressorial adhesion was greatly reduced (Fig. 4b), which indicates that ER stress, as per the loss of *SPS1*, reduced appressorial adhesion and abolished penetration. Third, when the antioxidant ascorbic acid was added to spores in amounts that do not affect appressorium formation[31], it remediated Δ*sps1* appressorial adhesion in 96-well plates (Fig. 4c) and restored Δ*sps1* appressorial penetration on rice leaf sheath surfaces (Fig. 4d and quantified in Extended Data Fig. 6b) due to restored appressorial mucilage production (Fig. 4e). We concluded that spermine is required to maintain the redox balance in the ER lumen in order to mitigate ROS-induced ER stress and facilitate glycoprotein folding and mucilage secretion for appressorial adhesion and subsequent cuticle penetration. The notion that ROS impairs glycoprotein folding and triggers ER stress, rather than ER stress resulting in elevated ROS, is supported by the data presented in Extended Data Fig. 6c, which shows how ascorbic acid did not remediate WT appressorial adhesion following Tun treatment at 6 h.p.i. Whether non-proteinaceous components of mucilage are still effectively secreted by the Δ*sps1* mutant is not known, but if so, the absence or reduction of the glycoprotein matrix must render the resulting composition ineffectual for appressorial adhesion.

The appressorium is a highly oxidative environment[6]. ROS produced by NOXs are required for cell wall crosslinking[6] and F-actin reorganization[3], but we wondered whether, in the absence of sperm-

ine, off-target and/or compartmentalized ROS might be a source of ER stress, as has been reported in vascular smooth muscle cells, where NOX1 ROS production contributes to protein hyperoxidation and ER stress[26,32]. If so, deleting *NOX* genes in Δ*sps1* might remediate appressorial mucilage secretion and adhesion. Δ*nox1* mutants, similar to Δ*sps1*, progress through appressorial development stages to form penetration pegs that fail to elongate into primary hyphae[3]. Thus, *NOX1* is unlikely to act upstream of *SPS1* and might provide useful epistatic information when deleted in Δ*sps1*, whereas Δ*nox2* mutants do not form penetration pegs[3], and results from Δ*sps1*Δ*nox2* double mutants might be harder to interpret. We generated the Δ*sps1*Δ*nox1* double mutant and found that although it could not (as expected) form functional penetration pegs on rice leaf sheaths, Δ*sps1*Δ*nox1* appressoria were restored for adhesion (Fig. 4f) and mucilage production (Fig. 4g) compared with the Δ*sps1* single-mutant strain. These results suggest that at least one source of ER stress in the absence of spermine might be off-target ROS from NADPH oxidase-1 (Nox1) in the ER lumen microcompartment.

Although there are no known reports in the literature that spermine has been detected in mucilages, including those of *M. oryzae*[18,22,23], it is nonetheless conceivable that spermine might be a component of mucilage or be directly required for mucilage assembly. However, considering that spermine is dispensable for Δ*sps1*Δ*nox1* appressorial mucilage secretion and adhesion, and that ascorbic acid treatment remediates Δ*sps1* adhesion, our results show that at best, spermine can only be a very minor, redundant or nonfunctional element of mucilage. Thus, on balance, we deem it unlikely that spermine is a component of *M. oryzae* appressorial mucilage.

To conclude, our results suggest that endogenous spermine precisely buffers off-target oxidative insults in the ER arising (at least in part) from Nox1-dependent ROS. This action facilitates glycoprotein folding and secretion that results in optimal appressorial mucilage production and tight adhesion followed by turgor buildup, successful penetration and host rice cell colonization. Consistent with the notion that spermine modulates ER ROS levels, we note that spermine acts directly as a free radical scavenger[7,27]. Furthermore, only spermine treatment remediated Δ*sps1* appressorial adhesion, and spermine was the only polyamine altered in concentration in Δ*sps1* mycelia, while Sps1 (but not the other polyamine biosynthetic enzymes) was predicted to localize to the ER and might provide a localized source of spermine for antioxidation purposes. Together, these results indicate that other polyamines do not have a role in ER stress remediation or adhesion. Considering that ROS generation at appressorial cell walls is nonetheless critical for appressorium development, and that treatments with high concentrations of the NOX inhibitor diphenyleneiodonium or the antioxidant ascorbic acid inhibit appressorium formation at germ tube tips[6,31], our findings might explain why germinating spores treated with exogenous spermine—which would similarly neutralize all ROS indiscriminately—fail to form appressoria[8] compared with spores loaded with endogenous or environmental spermine during conidiogenesis. Our results presented here provide a molecular mechanism of plant infection that is potentially targetable and likely to be broadly applicable to host–microbe interactions across taxa.

Methods

Strains and culture conditions. The strains used and generated during the course of this study are listed in Supplementary Table 2. The *M. oryzae* Guy11 isolate and a strain of Guy11 expressing histone H1 fused to RFP were used as parental strains where indicated. Strains were either grown on CM containing 1% (w/v) glucose, 0.2% (w/v) peptone, 0.1% (w/v) yeast extract and 0.1% (w/v) casamino acids or on glucose minimal media (GMM)[31]. Spore counts were made by collecting spores from 12-day-old CM plates. Radial growth was tested on CM plates and on GMM with 1% (w/v) glucose and 55 mM nitrate as the sole carbon and nitrogen source, respectively. Agar plugs (5 mm in diameter) of WT and mutant strains were placed on CM or GMM. Plates were grown at 24 °C with 12-h light–dark cycles. Images were taken of all plates at 10 days of growth using a Sony Cyber-shot digital camera (14.1 megapixels).

Gene functional analysis. Gene functional analysis involved targeted gene disruption of *SPS1* by homologous recombination using our standard split marker method[10]. A total of 507 base pairs of the *SPS1* sequence were replaced by the *ILV1* gene, which confers resistance to sulfonylurea[10]. One Δ*sps1* deletant was complemented with the full-length *SPS1* sequence under its native promoter to give the Δ*sps1 SPS1* complementation strain. The *SPS1*-carrying vector was constructed using the yeast GAP-repair method, as described by Zhou and colleagues[33]. *SPS1* was also deleted from the Δ*nox1* mutant strain[6] by replacing 507 base pairs of the *SPS1* coding sequence with a marker gene selective for hygromycin resistance (*hph*)[10]. Primers for constructing the strains used in this study are listed in Supplementary Table 3.

Phylogenetic analysis. The alignments and phylogenetic tree construction were performed using the online tool available at http://www.phylogeny.fr/ using the "One Click Mode" option. *M. oryzae* is annotated in the BLAST database as *Pyricularia oryzae*. The BLAST search retrieved 47 taxa among the 50 best hits.

Metabolomics analysis. Strains were grown on liquid CM for 48 h. Mycelia were collected in triplicate and lyophilized for 36 h. Approximately 30 mg of lyophilized mycelia was suspended in 1 ml of 80% methanol containing 2 μM $^{13}C_5$-^{15}N-proline as the injection standard. Samples were disrupted using a bullet blender (3 cycles of 4 min each) with 50 mg of ZrO beads per sample. After centrifugation, supernatants were removed and dried at 4 °C. Pellets were dissolved in 100 μl of 80% methanol, placed in vials at 4 °C and analysed by LC–MRM mass spectrometry (Sciex 4000 QTrap). A single transition was monitored per metabolite in each positive and negative mode (in separate injections). The chromatograms were analysed using the program Multiquant 3.0 from Sciex. Confirmation of the peak assignments was done against 40 metabolites in positive mode and 20 metabolites in negative mode. Metabolomic data normalization and analyses were performed using Metaboanalyst 3.0 (refs. [34,35]).

Pathogenicity tests and live-cell imaging. Fungal spores were collected from 12–14-day-old plates and suspended at a concentration of 1×10^5 spores per ml in 0.2% gelatin (Difco). Whole-plant infection assays were performed by spraying 10 ml of the spore suspension onto 3–4-week-old rice (*Oryza sativa*) seedlings of the susceptible cultivar CO-39. Infected plants were kept in the dark overnight and then transferred to a growth chamber with 12-h light–dark periods at 26 °C. Abraded leaf inoculations were performed by wounding detached rice leaves with an inoculation needle and placing a mycelial plug with the respective WT or Δ*sps1* strain on top of the damaged area. Lesion formation was examined at 120 h.p.i., and images of the infected leaves were taken using an Epson Perfection V550 scanner at a resolution of 600 dots per inch.

Detached rice leaf sheaths, prepared as previously described[31], were inoculated with 1×10^5 spores per ml collected from CM, or from CM supplemented with the indicated polyamines, repeated in triplicate. Appressoria formation rates were calculated at 24 h.p.i. from 50 spores per leaf sheath, repeated in triplicate. Penetration rates were calculated at 30 h.p.i. from the number of IH emerging from 50 appressoria per leaf sheath, repeated in triplicate. After leaf sheaths were trimmed, live-cell imaging was performed using a Nikon A1 confocal laser scanning microscope mounted on a Nikon 90i compound microscope at the University of Nebraska-Lincoln Morrison Microscopy Core Research Facility. CFW fluorescence was detected at 425–475 nm. tdTomato fluorescence was detected at 570–620 nm. CFW excitation was detected at 405 nm. tdTomato excitation was detected at 561 nm. All confocal images were processed using the software NIS-Elements 4.40.00. All microscopy images were analysed using ImageJ v.2.0

Appressorium formation and turgor measurement. Appressorium development was evaluated by live-cell imaging on both artificial hydrophobic surfaces (plastic coverslips or cellophane) and on rice leaf sheath surfaces following inoculation with 1×10^5 spores per ml. Cell cycle progression and autophagy were assessed by observing the number of nuclei carried in spores and appressoria of H1:RFP strains at the indicated time points. Appressorial cell walls were stained using 0.02% (w/v) CFW (Sigma Aldrich). Nitrotetrazolium blue chloride (0.3 mM; ThermoFisher) was used to detect ROS accumulation in appressoria at 24 h.p.i.

Appressorial turgor pressure and cell wall porosity were evaluated as previously described[36]. The generation of turgor pressure by both WT and mutant strains was estimated by counting the number of appressoria undergoing cytorrhysis at 24 h.p.i., characterized by the collapse of the appressorium, after treatment with increasing concentrations of glycerol (1–4 M). Appressorial porosity was estimated by subjecting appressoria of WT and Δ*sps1* to different molecular weights of PEG solutions (PEG 400, PEG 1000, PEG 4000 and PEG 8000) to produce a constant osmotic pressure of 4 MPa. Glycerol at 4 Mpa was used as a control. Subsequently, the ratio of plasmolysis to cytorrhysis was calculated.

Appressorial adhesion assay. Appressorial adhesion rates were evaluated in 96-well ELISA plates (ThermoFisher) as previously described[19,20]. Wells were

inoculated at a rate of 1×10^4 spores per ml and incubated at 26 °C. At 24 h.p.i., wells were washed three times by submersion in sterile distilled water. After air-drying, 100 µl of 0.05% (w/v) crystal violet (Sigma-Aldrich) was added to each well and the plates incubated at room temperature for 20 min. The plates were then washed three times with sterile distilled water and air-dried. Ethanol (98%; 100 µl) was added to each well and the plate was shaken at room temperature for 15 min. The absorbance was measured at 570 nm on a BioTek Microplate spectrophotometer using the manufacturer's recommendations. Values were compared against controls, which were air-dried but not washed at 24 h.p.i., to provide a percentage value of appressorial adhesion. Assays were performed with three biological replicates, each read in triplicate.

SEM analysis. Appressoria were formed on rice leaf sheaths for 24 h. Samples were fixed in 2.5% glutaraldehyde, subjected to post-fixation with 1% osmium tetroxide, followed by series dehydration in ethanol and acetone. Appressoria formed on cellophane membranes were placed on top of a 3% (w/v) water–agar substrate for 48 h to air-dry before examining intact appressoria and mucilage, or following sonication for 30 min. All samples were placed on a double-sided adhesive conductive tab on an aluminium SEM sample-mounting stub. Samples were sputter coated with chromium (~5-nm thick) using a Denton Vacuum Desk V sputter coater and imaged on a Hitachi S-4700 field emission scanning electron microscope at ×5,000 and ×10,000 magnifications.

TEM analysis. Appressoria were formed on hydrophobic cover slips. Samples were fixed in 2.5% glutaraldehyde, subjected to post fixation with 1% osmium tetroxide, followed by series dehydration in ethanol and acetone. Samples were embedded in blocks using a Low Viscosity Embedding Media Spurr's kit (Electron Microscopy Sciences). Sections (100-nm thick) were cut on a Leica EM UC7 Ultramicrotome. Sections were stained using uranyl acetate and lead citrate. All sample grids were imaged on a Hitachi H7500 transmission electron microscope at ×10,000 magnifications.

Statistics and reproducibility. All values represent the mean of three biological replicates unless otherwise stated. Sample sizes were chosen based on previous studies in the field[10,31]. Error bars indicate the standard deviation. Statistical comparisons were performed using one-way or two-way analysis of variance (ANOVA) and unpaired two-tailed *t*-test ($P < 0.05$) available in GraphPad Prism (v.8-4). Confocal and SEM images are representative of at least three biological replications. TEM images are representative of 150 appressoria per strain on three independent slides.

Reporting Summary. Further information on research design is available in the Nature Research Reporting Summary linked to this article.

Data availability

The *M. oryzae SPS1* gene sequence is available at NCBI under the accession MGG_01296. Data supporting the findings of this study are available from the corresponding author upon request. Mutant strains generated during the course of this study are available from the corresponding author upon request and with an appropriate APHIS permit. Numerical and statistical source data that underlie the graphs in figures and extended data are provided with the paper.

Received: 22 April 2020; Accepted: 4 August 2020;
Published online: 14 September 2020

References

1. Wilson, R. A. & Talbot, N. J. Under pressure: investigating the biology of plant infection by *Magnaporthe oryzae*. *Nat. Rev. Microbiol.* **7**, 185–195 (2009).
2. Howard, R. J. & Valent, B. Breaking and entering: host penetration by the fungal rice blast pathogen *Magnaporthe grisea*. *Annu. Rev. Microbiol.* **50**, 491–512 (1996).
3. Ryder, L. S. et al. NADPH oxidases regulate septin-mediated cytoskeletal remodeling during plant infection by the rice blast fungus. *Proc. Natl Acad. Sci. USA* **110**, 3179–3184 (2013).
4. Ryder, L. S. et al. A sensor kinase controls turgor-driven plant infection by the rice blast fungus. *Nature* **574**, 423–427 (2019).
5. Sun, G., Elowsky, C., Li, G. & Wilson, R. A. TOR-autophagy branch signaling via Imp1 dictates plant–microbe biotrophic interface longevity. *PLoS Genet.* **14**, e1007814 (2018).
6. Egan, M. J., Wang, Z. Y., Jones, M. A., Smirnoff, N. & Talbot, N. J. Generation of reactive oxygen species by fungal NADPH oxidases is required for rice blast disease. *Proc. Natl Acad. Sci. USA* **104**, 11772–11777 (2007).
7. Rocha, R. O. & Wilson, R. A. Essential, deadly, enigmatic: polyamine metabolism and roles in fungal cells. *Fungal Biol. Rev.* **33**, 47–57 (2019).
8. Choi, W. B., Kang, S. H., Lee, Y. W. & Lee, Y. H. Cyclic AMP restores appressorium formation inhibited by polyamines in *Magnaporthe grisea*. *Phytopathology* **88**, 58–62 (1998).
9. Dean, R. A. et al. The genome sequence of the rice blast fungus *Magnaporthe grisea*. *Nature* **434**, 980–986 (2005).
10. Wilson, R. A., Gibson, R. P., Quispe, C. F., Littlechild, J. A. & Talbot, N. J. An NADPH-dependent genetic switch regulates plant infection by the rice blast fungus. *Proc. Natl Acad. Sci. USA* **107**, 21902–21907 (2010).
11. Hamasaki-Katagiri, N., Katagiri, Y., Tabor, C. W. & Tabor, H. Spermine is not essential for growth of *Saccharomyces cerevisiae*: identification of the *SPE4* gene (spermine synthase) and characterization of a *spe4* deletion mutant. *Gene* **210**, 195–201 (1998).
12. Saunders, D. G., Aves, S. J. & Talbot, N. J. Cell cycle-mediated regulation of plant infection by the rice blast fungus. *Plant Cell* **22**, 497–507 (2010).
13. Veneault-Fourrey, C., Barooah, M., Egan, M., Wakley, G. & Talbot, N. J. Autophagic fungal cell death is necessary for infection by the rice blast fungus. *Science* **312**, 580–583 (2006).
14. Kershaw, M. J. & Talbot, N. J. Genome-wide functional analysis reveals that infection-associated fungal autophagy is necessary for rice blast disease. *Proc. Natl Acad. Sci. USA* **106**, 15967–15972 (2009).
15. Marroquin-Guzman, M., Sun, G. & Wilson, R. A. Glucose–*ABL1*–TOR signaling modulates cell cycle tuning to control terminal appressorial cell differentiation. *PLoS Genet.* **13**, e1006557 (2017).
16. Sun, G., Qi, X. & Wilson, R. A. A feed-forward subnetwork emerging from integrated TOR- and cAMP/PKA-signaling architecture reinforces *Magnaporthe oryzae* appressorium morphogenesis. *Mol. Plant Microbe Interact.* **32**, 593–607 (2019).
17. Howard, R. J., Ferrari, M. A., Roach, D. H. & Money, N. P. Penetration of hard substrates by a fungus employing enormous turgor pressures. *Proc. Natl Acad. Sci. USA* **88**, 11281–11284 (1991).
18. Ebata, Y., Yamamoto, H. & Uchiyama, T. Chemical composition of the glue from appressoria of *Magnaporthe grisea*. *Biosci. Biotechnol. Biochem.* **62**, 672–674 (1998).
19. O'Toole, G. A. et al. Genetic approaches to the study of biofilms. *Methods Enzymol.* **310**, 91–109 (1999).
20. Skamnioti, P. & Gurr, S. J. *Magnaporthe grisea* cutinase2 mediates appressorium differentiation and host penetration and is required for full virulence. *Plant Cell* **19**, 2674–2689 (2007).
21. Galloway, A. F., Knox, P. & Krause, K. Sticky mucilages and exudates of plants—putative microenvironmental design elements with biotechnological value. *New Phytol.* **225**, 1461–1469 (2020).
22. Inoue, K., Onoe, T., Park, P. & Ikeda, K. Enzymatic detachment of spore germlings in *Magnaporthe oryzae*. *FEMS Microbiol. Lett.* **323**, 13–19 (2011).
23. Inoue, K. et al. Extracellular matrix of *Magnaporthe oryzae* may have a role in host adhesion during fungal penetration and is digested by matrix metalloproteinases. *J. Gen. Plant Pathol.* **73**, 388–398 (2007).
24. Tu, B. P. & Weissman, J. S. Oxidative protein folding in eukaryotes: mechanisms and consequences. *J. Cell Biol.* **164**, 341–346 (2004).
25. Wang, Q., Groenendyk, J. & Michalak, M. Glycoprotein quality control and endoplasmic reticulum stress. *Molecules* **20**, 13689–13704 (2015).
26. Santos, C. X. et al. Endoplasmic reticulum stress and Nox-mediated reactive oxygen species signaling in the peripheral vasculature: potential role in hypertension. *Antioxid. Redox. Signal* **20**, 121–134 (2014).
27. Ha, H. C. et al. The natural polyamine spermine functions directly as a free radical scavenger. *Proc. Natl Acad. Sci. USA* **95**, 11140–11145 (1998).
28. Smirnova, O. A., Bartosch, B., Zakirova, N. F., Kochetkov, S. N. & Ivanov, A. V. Polyamine metabolism and oxidative protein folding in the ER as ROS-producing systems neglected in virology. *Int. J. Mol. Sci.* **19**, 1219 (2018).
29. Yi, M. et al. The ER chaperone LHS1 is involved in asexual development and rice infection by the blast fungus *Magnaporthe oryzae*. *Plant Cell* **21**, 681–695 (2009).
30. Qi, Z. et al. The syntaxin protein (MoSyn8) mediates intracellular trafficking to regulate conidiogenesis and pathogenicity of rice blast fungus. *New Phytol.* **209**, 1655–1667 (2016).
31. Marroquin-Guzman, M. et al. The *Magnaporthe oryzae* nitrooxidative stress response suppresses rice innate immunity during blast disease. *Nat. Microbiol.* **2**, 17054 (2017).
32. Camargo, L. L. et al. Vascular Nox (NADPH oxidase) compartmentalization, protein hyperoxidation, and endoplasmic reticulum stress response in hypertension. *Hypertension* **72**, 235–246 (2018).
33. Zhou, X., Li, G. & Xu, J. R. Efficient approaches for generating GFP fusion and epitope-tagging constructs in filamentous fungi. *Methods Mol. Biol.* **722**, 199–212 (2011).
34. Xia, J., Sinelnikov, I. V., Han, B. & Wishart, D. S. MetaboAnalyst 3.0—making metabolomics more meaningful. *Nucleic Acids Res.* **43**, W251–W257 (2015).
35. Xia, J. & Wishart, D. S. Using MetaboAnalyst 3.0 for comprehensive metabolomics data analysis. *Curr. Protoc. Bioinformatics* **55**, 14.10.1–14.10.91 (2016).
36. Goh, J. et al. The PEX7-mediated peroxisomal import system is required for fungal development and pathogenicity in *Magnaporthe oryzae*. *PLoS ONE* **6**, e28220 (2011).

Acknowledgements

We thank Y. Zhou and J. Russ of the UNL Microscopy Core facility for SEM and TEM imaging. We thank J. Seravalli, UNL Redox Biology Center, for LC–MRM mass spectrometry. We thank H. Appeah, UNL, for technical assistance. We thank D. S. Carvalho and A. Góes-Neto, Federal University of Minas Gerais, Brazil, for assistance with the phylogenetic analysis. We thank N. J. Talbot, The Sainsbury Laboratory, UK, for the gift of Δ*nox1*. This work was supported by a National Science Foundation award to R.A.W. through the Plant Biotic Interactions program (IOS-1758805). R.O.R. was supported by a Capes scholarship/Science without Borders/Process number 99999.009138/2013-07 award. N.T.T.P. was supported by a UNL UCARE scholarship.

Author contributions

R.A.W. conceptualized the study. R.A.W. acquired funding for the experiments. R.O.R. and R.A.W. conceived, designed and guided the study. R.O.R., C.E. and N.T.T.P. acquired and analysed the data. Specifically, R.O.R. generated the mutant strains and characterized them together with N.T.T.P; confocal microscopy was performed by R.O.R. and C.E.; and SEM and TEM analyses were performed by R.O.R. The appressorial adhesion assays were performed by R.O.R. R.O.R. and R.A.W. interpreted the data. R.O.R. and R.A.W. wrote the first draft of the paper. R.A.W. wrote the final draft of the paper.

Competing interests

The authors declare no competing interests.

Additional information

Extended data is available for this paper at https://doi.org/10.1038/s41564-020-0786-x.

Supplementary information is available for this paper at https://doi.org/10.1038/s41564-020-0786-x.

Correspondence and requests for materials should be addressed to R.A.W.

Reprints and permissions information is available at www.nature.com/reprints.

Publisher's note Springer Nature remains neutral with regard to jurisdictional claims in published maps and institutional affiliations.

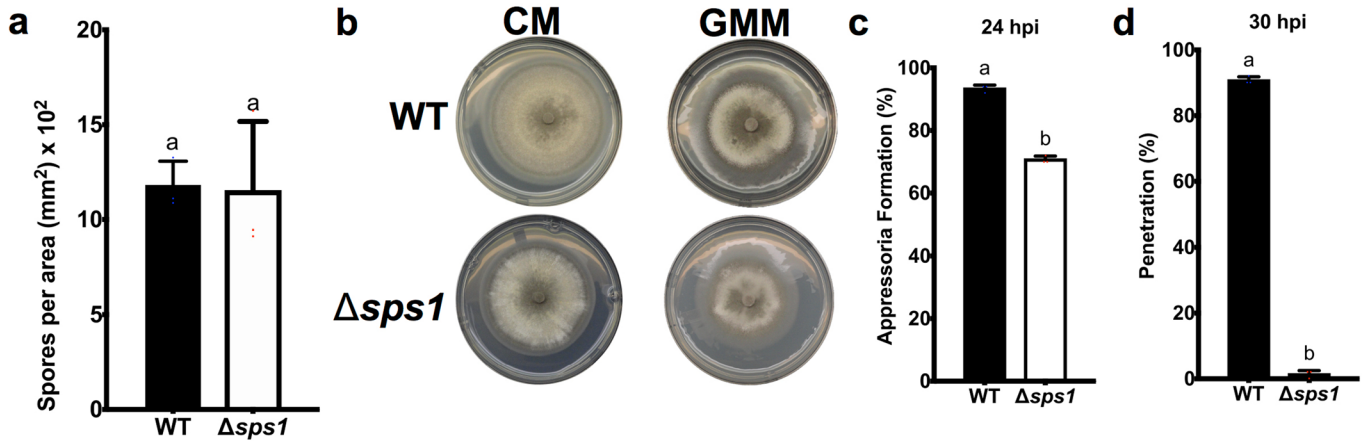

Extended Data Fig. 1 | Δ*sps1* physiology compared to WT. a, Sporulation rates of WT and the Δ*sps1* mutant strains were not significantly different (unpaired two-tailed t-test, t = 0.1346 df = 4, $p = 0.8994$) following 14 days of growth on CM. Value are the mean of spores liberated from three independent plates. Bars are standard deviation. **b**, WT and Δ*sps1* strains after ten days of growth on 88 mm petri-dishes containing complete media (CM) or 1 % (w/v) glucose minimal media (GMM), as indicated. Three independent plate test experiments gave similar results. **c**, Appressorium formation rates on detached rice leaf sheath surfaces. Values are means obtained by determining how many of n=50 germinating conidia had formed appressoria by 24 h.p.i., repeated in triplicate. Bars are standard deviation. Bars with different letters are significantly different (unpaired two-tailed t-test, t = 24.04, df = 4, $p < 0.0001$). **d**, Appressorial penetration rates on detached rice leaf sheaths. Values are means obtained by determining how many of n=50 appressoria had penetrated rice cuticles by 30 h.p.i., as determined by observing primary hyphae or early IH in underlying rice cells, repeated in triplicate. Bars are standard deviation. Bars with different letters are significantly different (unpaired two-tailed t-test, t = 94.75 df = 4, $p < 0.0001$). **c**, **d**, Leaf sheaths were inoculated with 1 x 10^5 spores per mL of the indicated strain.

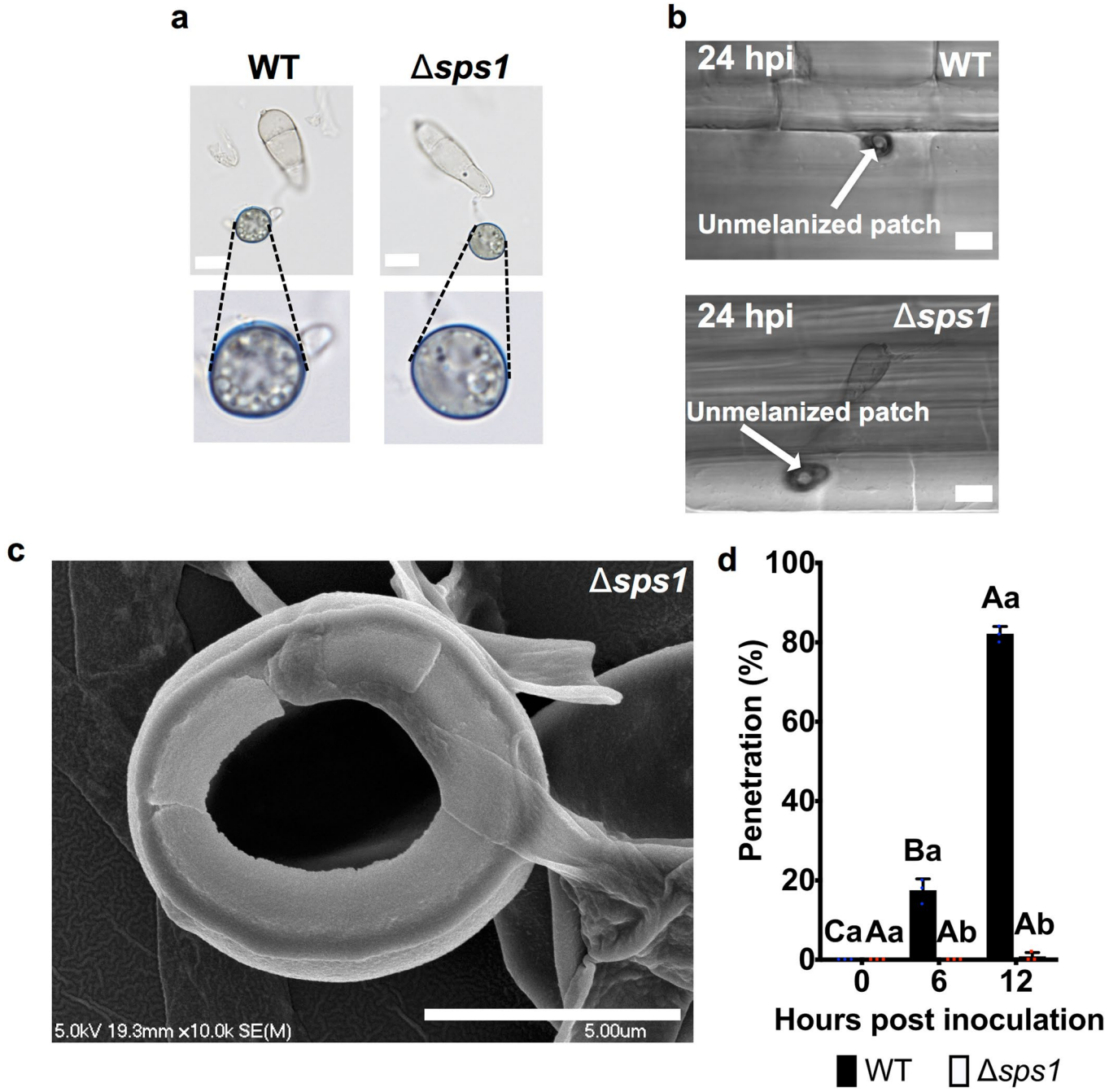

Extended Data Fig. 2 | Appressorial developmental processes prior to penetration are not affected by *SPS1* deletion. a, Superoxide detection by nitrotetrazolium blue chloride (NBT) staining shows Δ*sps1* appressoria generated reactive oxygen species (ROS) at the appressorial cell wall like WT. Samples were stained with 0.3 mM NBT at 24 h.p.i. for one hour before imaging. Images are representative of three experiments performed on plastic cover slips. **b**, Live-cell imaging of detached rice leaf sheaths by bright field microscopy shows unmelanized patches covering the pore at the base of both WT and Δ*sps1* appressoria. Scale bar is 10 μm. Images are representative of three experiments. **c**, Δ*sps1* appressoria on cellophane were dislodged at 24 h.p.i. by sonication for 30 min. In this example, the liberated appressorium has been flipped upside down, revealing a perfectly formed appressorial pore. Scale bar is 5 μm. **d**, Penetration rates of Δ*sps1* and WT appressoria at 24 h.p.i. after treatment with 2.5 mM spermine at the indicated time points. Values are the mean penetration rates determined for n=50 appressoria, repeated in triplicate. Bars are standard deviation. Significant differences of the means comparing WT and Δ*sps1* at a given treatment are denoted by different lowercase letters (two-way ANOVA, $F_{2, 12} = 1126$, $p < 0.0001$). Significant differences of the means within WT (one-way ANOVA, $F_{2, 6} = 1261$, $p < 0.0001$) or within Δ*sps1* (one-way ANOVA, $F_{2, 6} = 1.00$, $p = 0.42$) at different treatments are denoted by different uppercase letters.

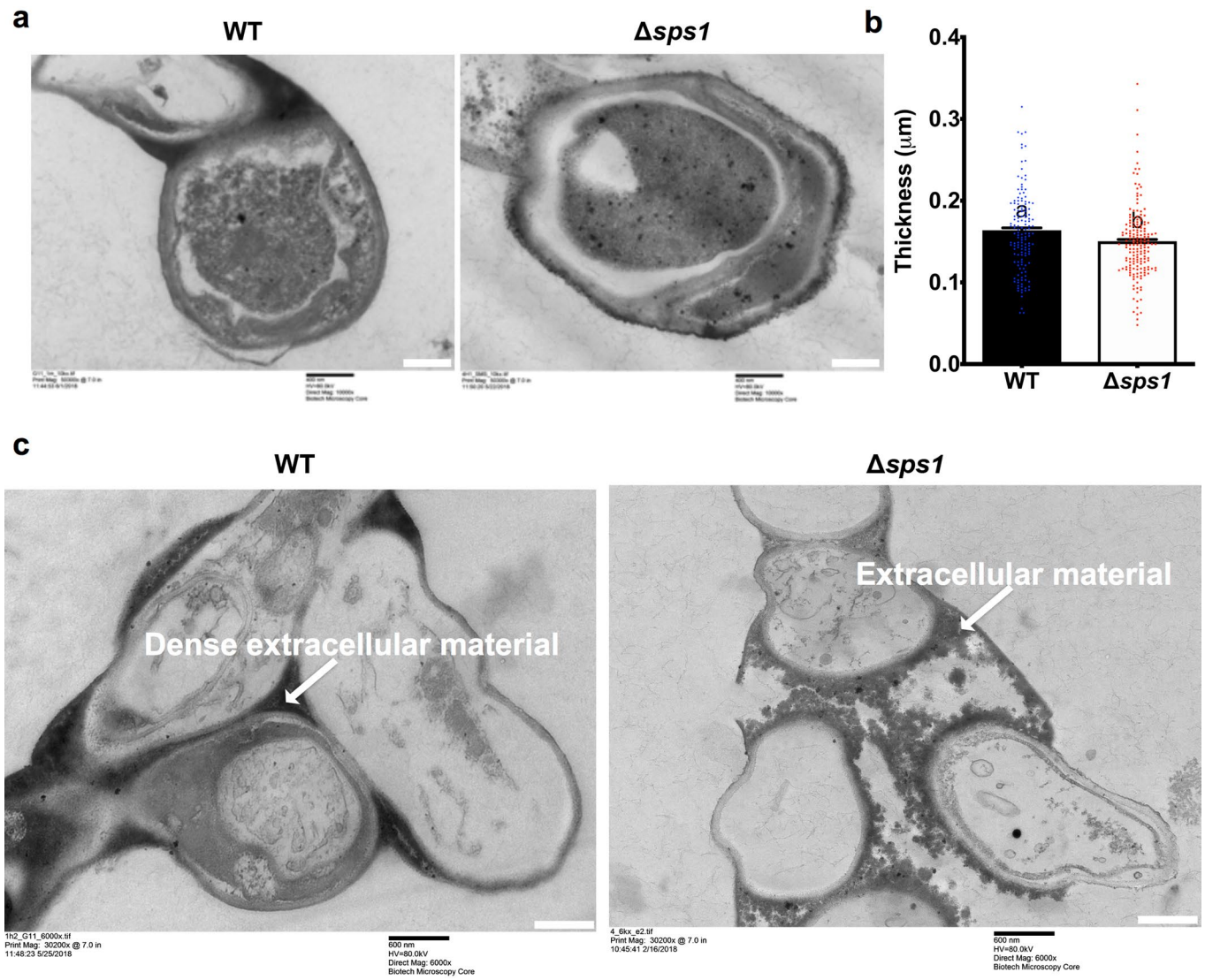

Extended Data Fig. 3 | *SPS1* deletion affects appressorial cell wall shape and thickness and mucilage production. a, Transmission electron microscopy (TEM) of Δ*sps1* and WT appressoria on plastic coverslips. Scale bar is 400 nm. **b**, Measurements of appressorial cell wall thickness after TEM. Values are the mean ± standard deviation of measurements from appressoria (n=144 for WT and n=174 for Δ*sps1*) . Significant differences of means comparing WT and Δ*sps1* at the given treatment are denoted by different letters (unpaired two-tailed t-test, t = 2.580 df = 316, $p = 0.0103$). **c**, TEM of Δ*sps1* and WT appressoria on plastic coverslips at 24 h.p.i. showing examples of extracellular secretions, likely mucilage, that are sparser in Δ*sps1* than WT samples. Scale bar is 600 nm.

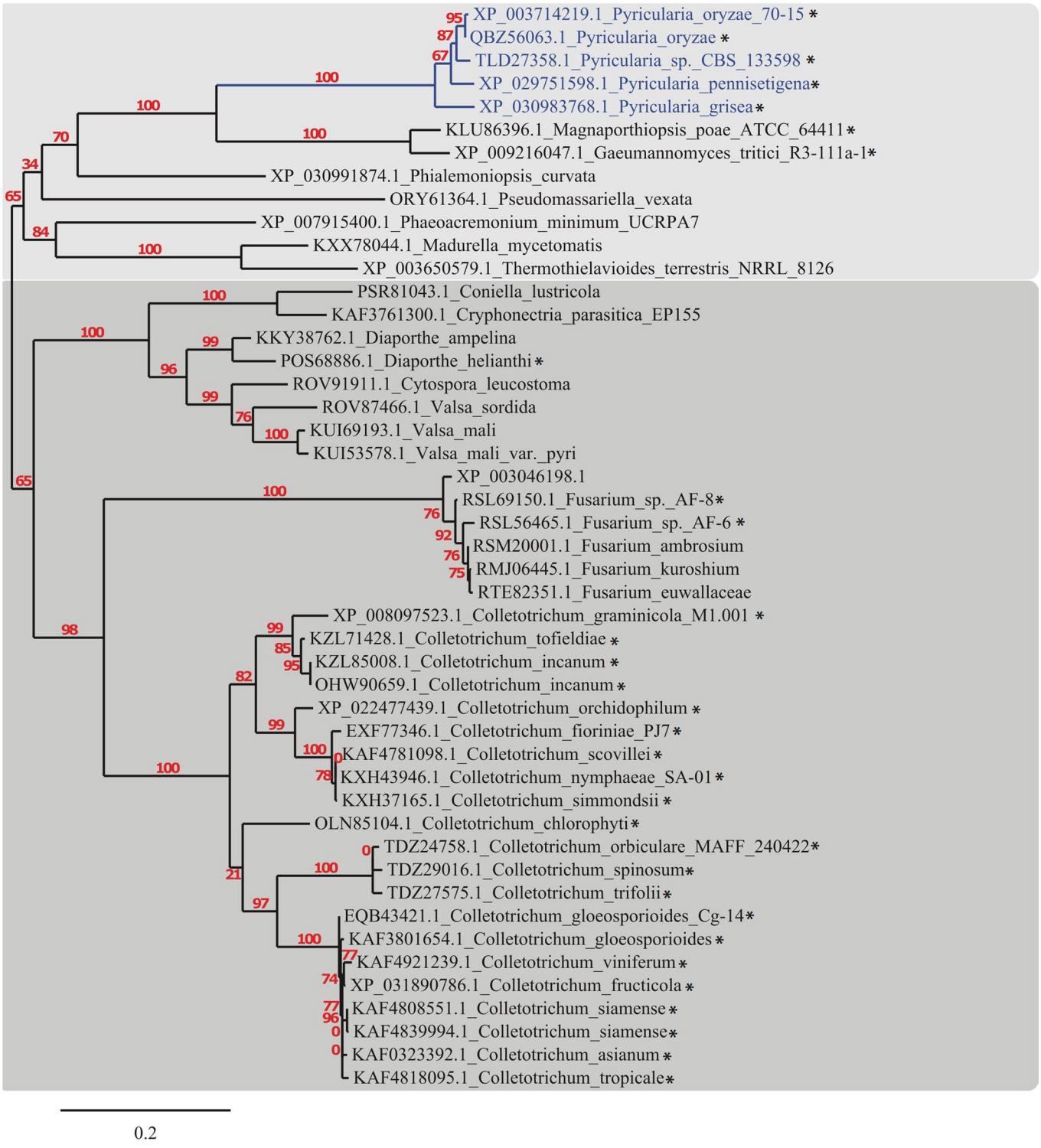

Extended Data Fig. 4 | *SPS1* homologues are present in the genomes of other filamentous fungi including those that form appressoria or appressoria-like infection structures. Unrooted maximum likelihood phylogenetic tree shows two main clusters of species carrying Sps1 homologues (light gray and dark gray). Branches of *M. oryzae* (syn. *Pyricularia oryzae*) and related species of Pyricularia (magnaporthe-like sexual morphs) are shown in blue. Values represent the support percentage for each branch. Branch length scale is shown in the bottom left. Asterisks indicate species that form appressoria or appressoria-like structures.

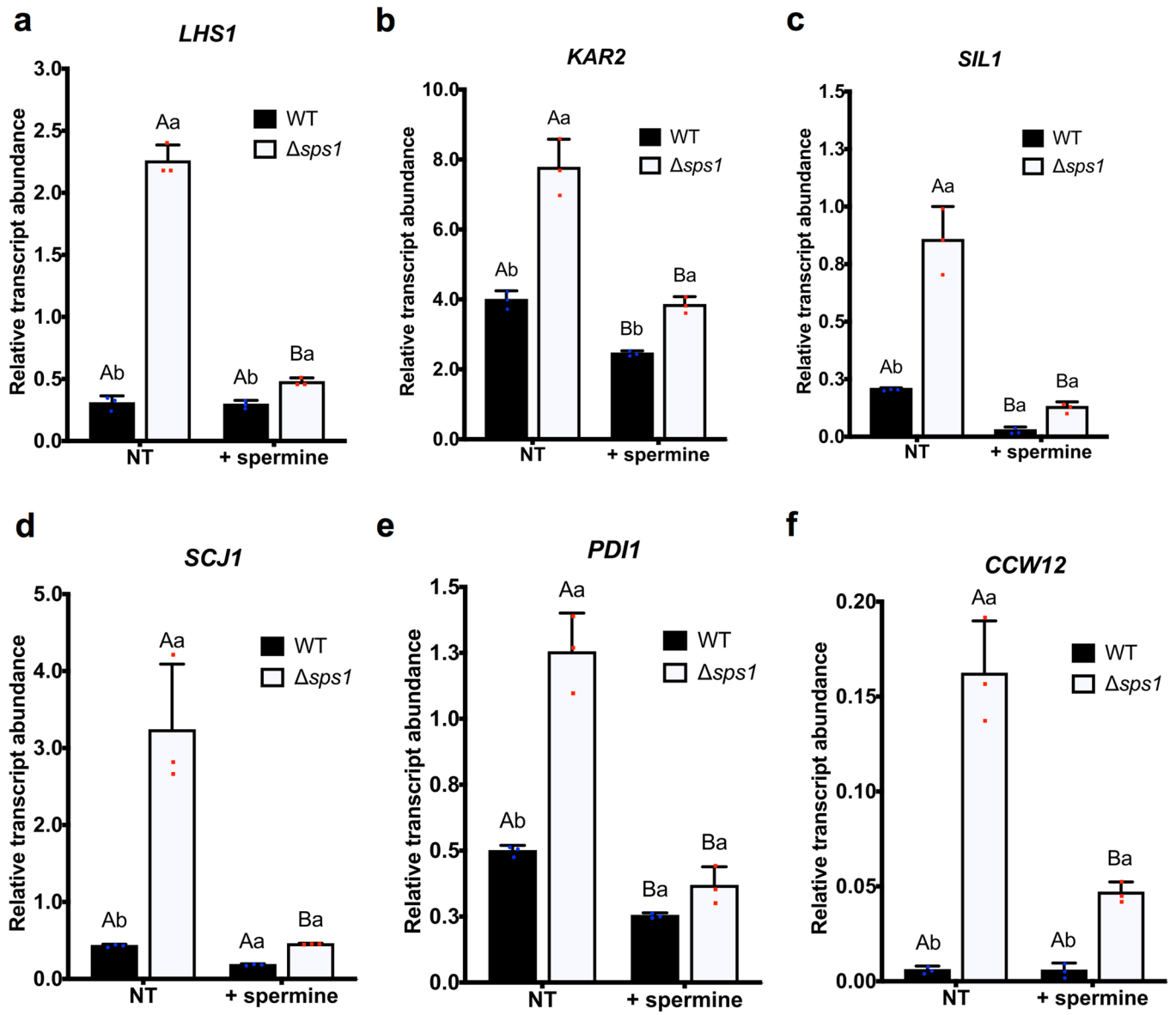

Extended Data Fig. 5 | Loss of spermine induces the unfolded protein response (UPR) and cell wall integrity (CWI) response. ER stress induces the UPR and CWI. Relative transcript abundances of UPR-associated genes (*LHS1*, *KAR2*, *SCJ1*, *SIL1*, *PDI1*)[29] and a cell wall integrity-associated gene (*CCW12*)[30] were upregulated in the Δ*sps1* strain grown in liquid complete media without spermine supplementation compared to WT. Levels of the indicated genes were reduced in Δ*sps1* mycelia when grown in the presence of 1 mM spermine. Expression levels were normalized against *M. oryzae* β-tubulin gene expression. Quantitative real-time PCR assays were carried out in triplicate. Template controls did not show amplification. Error bars indicate standard deviation. Significant differences of the means comparing WT and Δ*sps1* at the indicated treatment are denoted by different lowercase letters (two-way ANOVA, ***LHS1*** $F_{1,8} = 432.9$. NT, $p < 0.0001$. + Spermine, $p = 0.0327$; ***KAR2*** $F_{1,8} = 22.10$. NT, $p < 0.0001$. + Spermine, $p = 0.0096$; ***SIL1*** $F_{1,8} = 42.12$. NT, $p < 0.0001$. + Spermine, $p = 0.2416$; ***PDI1*** $F_{1,8} = 45.40$. NT, $p < 0.0001$. + Spermine, $p = 0.2443$; ***SCJ1*** $F_{1,8} = 26.42$. NT, $p < 0.0001$. + Spermine, $p = 0.7101$; ***CCW12*** $F_{1,8} = 49.28$. NT, $p < 0.0001$. + Spermine, $p = 0.0151$). Significant differences of the means within WT or within Δ*sps1* are denoted by different uppercase letters (two-way ANOVA, ***LHS1*** $F_{1,8} = 432.9$. WT, $p = 0.9781$. Δ*sps1*, $p < 0.0001$; ***KAR2*** $F_{1,8} = 22.10$. WT, $p = 0.0055$. Δ*sps1*, $p < 0.0001$; ***SIL2*** $F_{1,8} = 42.12$. WT, $p = 0.0328$. Δ*sps1*, $p < 0.0001$; ***PDI1*** $F_{1,8} = 45.40$. WT, $p = 0.0129$. Δ*sps1*, $p < 0.0001$; ***SCJ1*** $F_{1,8} = 26.42$. WT, $p = 0.7503$. Δ*sps1*, $p < 0.0001$; ***CCW12*** $F_{1,8} = 49.28$. WT, $p = 0.9996$. Δ*sps1*, $p < 0.0001$).

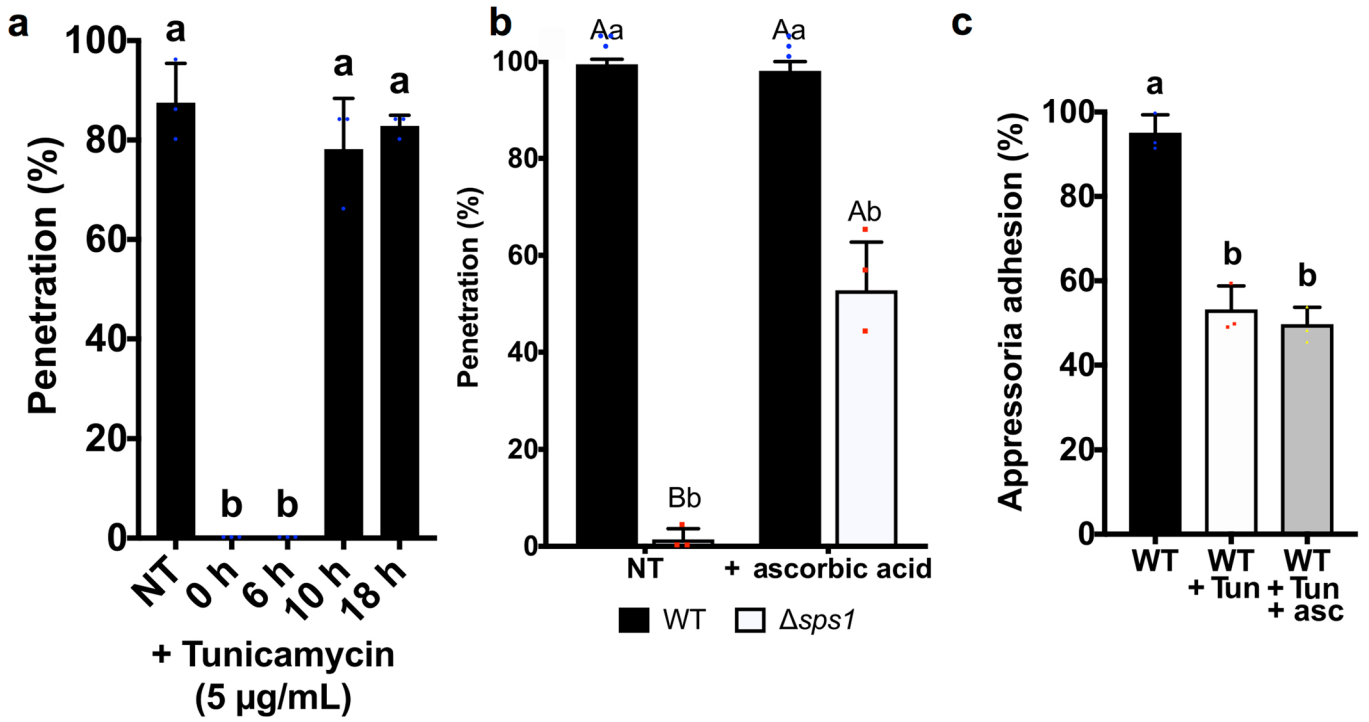

Extended Data Fig. 6 | Tunicamycin and ascorbic acid treatments affect appressorial penetration and adhesion. a, Penetration rates at 30 h.p.i. for appressoria formed on rice leaf sheath surfaces from germinating WT spores treated or untreated (NT) with Tunicamycin (5 µg/mL) at the indicated time points. Values are the mean penetration rates determined for n=50 appressoria, repeated in triplicate. Bars are standard deviation. Significant differences of the means at a given time are denoted by different lowercase letters (one-way ANOVA, $F_{4,10} = 173.00$, $p < 0.0001$). **b**, Penetration rates at 30 h.p.i. for appressoria formed on rice leaf sheath surfaces from spores treated with 0.25 µM ascorbic acid. NT, no treatment. Values are the mean penetration rates determined for n=50 appressoria, repeated in triplicate. Bars are standard deviation. Significant differences of the means comparing WT and Δ*sps1* at a given treatment are denoted by different lowercase letters (two-way ANOVA, $F_{1,8} = 74.30$. NT, $p < 0.0001$; + Ascorbic acid $p < 0.0001$). Significant differences of the means within WT or within Δ*sps1* are denoted by different uppercase letters (letters (two-way ANOVA, $F_{1,8} = 74.30$. WT, $p = 0.9450$; Δ*sps1*, $p < 0.0001$). **c**, Rates of WT appressorial adhesion in 96-well plates at 24 h.p.i. after germinating spores were treated at 6 h.p.i. with 2.5 µM ascorbic acid (asc) and/ or 5 µg/ mL Tunicamycin (Tun). This was repeated in triplicate for each treatment. Significant differences of the means are denoted by different lowercase letters (one-way ANOVA, $F_{2,6} = 80.35$, $p < 0.0001$). Error bars indicate standard deviation.

nature research

Corresponding author(s): Richard Wilson

Last updated by author(s): 7/27/2020

Reporting Summary

Nature Research wishes to improve the reproducibility of the work that we publish. This form provides structure for consistency and transparency in reporting. For further information on Nature Research policies, see Authors & Referees and the Editorial Policy Checklist.

Statistics

For all statistical analyses, confirm that the following items are present in the figure legend, table legend, main text, or Methods section.

n/a	Confirmed
☐	☒ The exact sample size (*n*) for each experimental group/condition, given as a discrete number and unit of measurement
☐	☒ A statement on whether measurements were taken from distinct samples or whether the same sample was measured repeatedly
☐	☒ The statistical test(s) used AND whether they are one- or two-sided *Only common tests should be described solely by name; describe more complex techniques in the Methods section.*
☒	☐ A description of all covariates tested
☒	☐ A description of any assumptions or corrections, such as tests of normality and adjustment for multiple comparisons
☐	☒ A full description of the statistical parameters including central tendency (e.g. means) or other basic estimates (e.g. regression coefficient) AND variation (e.g. standard deviation) or associated estimates of uncertainty (e.g. confidence intervals)
☐	☒ For null hypothesis testing, the test statistic (e.g. *F*, *t*, *r*) with confidence intervals, effect sizes, degrees of freedom and *P* value noted *Give P values as exact values whenever suitable.*
☒	☐ For Bayesian analysis, information on the choice of priors and Markov chain Monte Carlo settings
☒	☐ For hierarchical and complex designs, identification of the appropriate level for tests and full reporting of outcomes
☒	☐ Estimates of effect sizes (e.g. Cohen's *d*, Pearson's *r*), indicating how they were calculated

Our web collection on statistics for biologists contains articles on many of the points above.

Software and code

Policy information about availability of computer code

Data collection	Metabolomics was perfomed using LC-MRM Mass spectrometry (Sciex 4000 QTrap) and chromatograms were analyzed using Multiquant 3.0 from Sciex. Confocal images were taken by a Nikon 90i compound microscope. SEM and TEM images were taken by a Hitachi S-4700 Field Emission SEM and Hitachi H7500 TEM, respectively
Data analysis	All data were analyzed by GraphPad Prism 8-4. Metabolomic data were analyzed using Metaboanalyst 3.0. All confocal images were processed by the software NIS-Elements 4.40.00. All microscopy images were analyzed using ImageJ version 2.0.

For manuscripts utilizing custom algorithms or software that are central to the research but not yet described in published literature, software must be made available to editors/reviewers. We strongly encourage code deposition in a community repository (e.g. GitHub). See the Nature Research guidelines for submitting code & software for further information.

Data

Policy information about availability of data

All manuscripts must include a data availability statement. This statement should provide the following information, where applicable:

- Accession codes, unique identifiers, or web links for publicly available datasets
- A list of figures that have associated raw data
- A description of any restrictions on data availability

The Magnaporthe oryzae SPS1 gene sequence is available at NCBI under the accession MGG_01296. Data supporting the findings of this study are available from the corresponding author upon request.

Field-specific reporting

Please select the one below that is the best fit for your research. If you are not sure, read the appropriate sections before making your selection.

☒ Life sciences ☐ Behavioural & social sciences ☐ Ecological, evolutionary & environmental sciences

For a reference copy of the document with all sections, see nature.com/documents/nr-reporting-summary-flat.pdf

Life sciences study design

All studies must disclose on these points even when the disclosure is negative.

Sample size	Sample size was chosen according to long-term experience in biological and biochemical experimentation, for example following Marroquin-Guzman et al. 2017, Nature Microbiology. Pathogenicity-related assays were conducted according to published protocols.
Data exclusions	No data were excluded from analysis.
Replication	All experiments were performed in triplicate or with three biological replicates. All attempts at replicating the results were successful.
Randomization	Investigators did not perform randomization.
Blinding	Investigators were not blinded to group allocation during the experiments or to the outcome assessment.

Reporting for specific materials, systems and methods

We require information from authors about some types of materials, experimental systems and methods used in many studies. Here, indicate whether each material, system or method listed is relevant to your study. If you are not sure if a list item applies to your research, read the appropriate section before selecting a response.

Materials & experimental systems

n/a	Involved in the study
☒	☐ Antibodies
☒	☐ Eukaryotic cell lines
☒	☐ Palaeontology
☒	☐ Animals and other organisms
☒	☐ Human research participants
☒	☐ Clinical data

Methods

n/a	Involved in the study
☒	☐ ChIP-seq
☒	☐ Flow cytometry
☒	☐ MRI-based neuroimaging